9308 *Inorg. Chem.* **2009**, *48*, 9308–9315
DOI: 10.1021/ic901164r

Inorganic Chemistry
Article

Structures and Reactivity Patterns of Group 9 Metallocorroles

Joshua H. Palmer,[†] Atif Mahammed,[‡] Kyle M. Lancaster,[†] Zeev Gross,*[,‡] and Harry B. Gray*[,†]

[†]*Beckman Institute, California Institute of Technology, Pasadena, California 91125, and* [‡]*Schulich Faculty of Chemistry, Technion−Israel Institute of Technology, Haifa 32000, Israel*

Received June 17, 2009

Group 9 metallocorroles **1-M(PPh$_3$)** and **1-M(py)$_2$** [**M** = Co(III), Rh(III), Ir(III); **1** denotes the trianion of 5,10,15-tris-pentafluorophenylcorrole] have been fully characterized by structural, spectroscopic, and electrochemical methods. Crystal structure analyses reveal that average metal−N(pyrrole) bond lengths of the bis-pyridine metal(III) complexes increase from Co (1.886 Å) to Rh (1.957 Å)/Ir (1.963 Å); and the average metal−N(pyridine) bond lengths also increase from Co (1.995 Å) to Rh (2.065 Å)/Ir (2.059 Å). Ligand affinities for **1-M(PPh$_3$)** axial coordination sites increase dramatically in the order **1-Co(PPh$_3$) < 1-Rh(PPh$_3$) < 1-Ir(PPh$_3$)**. There is a surprising invariance in the **M(+/0)** reduction potentials within the five- and six-coordinate corrole series, and even between them; the average **M(+/0)** potential of **1-M(PPh$_3$)** is 0.78 V vs Ag/AgCl in CH_2Cl_2 solution, whereas that of **1-M(py)$_2$** is 0.70 V under the same conditions. Electronic structures of one-electron-oxidized **1-M(py)$_2$** complexes have been assigned by analysis of electron paramagnetic resonance spectroscopic measurements: oxidation is corrole-centered for **1-Co(py)$_2$** (g = 2.008) and **1-Rh(py)$_2$** (g = 2.003), and metal-centered for **1-Ir(tma)$_2$** (g_{zz} = 2.489, g_{yy} = 2.010, g_{xx} = 1.884, g_{av} = 2.128) and **1-Ir(py)$_2$** (g_{zz} = 2.401, g_{yy} = 2.000, g_{xx} = 1.937, g_{av} = 2.113).

Introduction

Systematic investigations of transition metal corrole complexes have accelerated recently because of major advances in synthetic methods.[1−3] Many of these complexes, especially of first-row transition metals, exhibit striking reactivity: iron(IV) derivatives remain the only non-copper catalysts for the aziridination of olefins by chloramine-T;[4] manganese(III) catalyzes oxygenations via observable (oxo)manganese(V);[5] chromium(III) mediates the aerobic oxidation of thiophenol to diphenyl disulfide;[6] and iron(I) and cobalt(I) corroles catalyze the reduction of carbon dioxide.[7] These reactivity patterns highlight the role of strong corrole σ-donation in the activation of low-valent metal centers.[8] This same electronic property, which accounts for the unusual stability of nitrido chromium(VI) and manganese(VI) complexes,[9] clearly is an important factor in metallocorrole-catalyzed processes.[10] Complexes of triarylcorroles with group 13−15 elements have been characterized as well, often with a focus on photophysical properties;[11] importantly, a gallium(III) corrole has been shown to be both an in vivo imaging agent and an anticancer drug candidate.[12] Second-row metallocorroles have not been investigated extensively, although there are reports of silver(III),[13] ruthenium(III),[14] and rhodium(III)

*To whom correspondence should be addressed. E-mail: chr10zg@tx.technion.ac.il (Z.G.), hbgray@caltech.edu (H.B.G.).

(1) (a) Gross, Z.; Galili, N.; Saltsman, I. *Angew. Chem., Int. Ed.* **1999**, *38*, 1427–1429. (b) Paolesse, R.; Jaquinod, L.; Nurco, D. J.; Mini, S.; Sagone, F.; Boschi, T.; Smith, K. M. *Chem. Commun.* **1999**, 1307–1308. (c) Gross, Z.; Galili, N.; Simkhovich, L.; Saltsman, I.; Botoshansky, M.; Blaser, D.; Boese, R.; Goldberg, I. *Org. Lett.* **1999**, *1*, 599–602. (d) Koszarna, B.; Gryko, D. T. *J. Org. Chem.* **2006**, *71*, 3707–3717.

(2) (a) Gryko, D. T. *J. Porphyrins Phthalocyanines* **2008**, *12*, 906. (b) Nardis, S.; Monti, D.; Paolesse, R. *Mini-Rev. Org. Chem.* **2005**, *2*, 355–372.

(3) (a) Aviv, I.; Gross, Z. *Chem. Commun.* **2007**, 1987–1999. (b) Goldberg, D. P. *Acc. Chem. Res.* **2007**, *40*, 626–634. (c) Gryko, D. T.; Fox, J. P.; Goldberg, D. P. *J. Porphyrins Phthalocyanines* **2004**, *8*, 1091–1105.

(4) Simkhovich, L.; Gross, Z. *Tetrahedron Lett.* **2001**, *42*, 8089–8092.

(5) (a) Gross, Z.; Golubkov, G.; Simkhovich, L. *Angew. Chem., Int. Ed.* **2000**, *39*, 4045–4047. (b) Golubkov, G.; Bendix, J.; Gray, H. B.; Mahammed, A.; Goldberg, I.; DiBilio, A. J.; Gross, Z. *Angew. Chem., Int. Ed.* **2001**, *40*, 2132–2134. (c) Mandimutsira, B. S.; Ramdhanie, B.; Todd, R. C.; Wang, H. L.; Zareba, A. A.; Czemuszewicz, R. S.; Goldberg, D. P. *J. Am. Chem. Soc.* **2002**, *124*, 15170–15171.

(6) Mahammed, A.; Gray, H. B.; Meier-Callahan, A. E.; Gross, Z. *J. Am. Chem. Soc.* **2003**, *125*, 1162–1163.

(7) Grodkowski, J.; Neta, P.; Fujita, E.; Mahammed, A.; Simkhovich, L.; Gross, Z. *J. Phys. Chem. A.* **2002**, *106*, 4772–4778.

(8) (a) Gross, Z.; Gray, H. B. *Comments Inorg. Chem.* **2006**, *27*, 61. (b) Hocking, R. K.; DeBeer George, S.; Gross, Z.; Walker, F. A.; Hodgson, K. O.; Hedman, B.; Solomon, E. I. *Inorg. Chem.* **2009**, *48*, 1678–1688.

(9) (a) Golubkov, G.; Gross, Z. *Angew. Chem., Int. Ed.* **2003**, *42*, 4507–4510. (b) Golubkov, G.; Gross, Z. *J. Am. Chem. Soc.* **2005**, *127*, 3258–3259.

(10) (a) Gross, Z.; Gray, H. B. *Adv. Synth. Catal.* **2004**, *346*, 165–170. (b) Mahammed, A.; Gross, Z. *Angew. Chem., Int. Ed.* **2006**, *45*, 6544–6547. (c) Agadjanian, H.; Weaver, J. J.; Mahammed, A.; Rentsendorj, A.; Bass, S.; Kim, J.; Dmochowski, I. J.; Margalit, R.; Gray, H. B.; Gross, Z.; Medina-Kauwe, L. K. *Pharm. Res.* **2006**, *23*, 367–377. (d) Haber, A.; Mahammed, A.; Fuhrman, B.; Volkova, N.; Coleman, R.; Hayek, T.; Aviram, M.; Gross, Z. *Angew. Chem., Int. Ed.* **2008**, *47*, 7896–7900.

(11) Flamigni, L.; Gryko, D. T. *Chem. Soc. Rev.* **2009**, *38*, 1635–1646.

(12) Agadjanian, H.; Ma, J.; Rensendorj, A.; Valluripalli, V.; Hwang, J. Y.; Mahammed, A.; Farkas, D. L.; Gray, H. B. *Proc. Natl. Acad. Sci. U.S.A.* **2009**, *106*, 6105–6110.

(13) Bruckner, C.; Barta, C. A.; Brinas, R. P.; Krause Bauer, J. A. *Inorg. Chem.* **2003**, *42*, 1673–1680.

(14) Simkhovich, L.; Luobeznova, I.; Goldberg, I.; Gross, Z. *Chem.—Eur. J.* **2003**, *9*, 201–208.

Published on Web 09/08/2009

derivatives, with the latter functioning as a catalyst in carbene-transfer reactions.[15] An (oxo)molybdenum(V) corrole also has been characterized.[16]

Third-row transition metal corroles are extremely rare, with fully characterized (oxo)Re(V) and Ir(III) compounds representing the only known oxidation states.[17,18] We predicted that trianionic corroles, on the basis of their ability to stabilize numerous metals in high oxidation states,[19] would greatly stabilize iridium(III) and that these derivatives would exhibit strikingly different redox properties than iridium(III) porphyrins or organoiridium(III) complexes such as $[Ir(ppy)_3]$ (ppy = 2-phenylpyridine, Figure 1). Indeed, Ir(III) corroles can be stabilized even by weakly donating axial ligands, whereas Ir(III) porphyrins are only stable when the metal is further coordinated by organometallic ligands [such as in (por)Ir(CO)Cl and (por)Ir-R, where por stands for the porphyrin dianion and R = alkyl or hydride)].[20]

A stable six-coordinate (tpfc)Ir(tma)$_2$ complex (**1-Ir(tma)$_2$**, Figure 1) was obtained via the reaction of $[Ir(cod)Cl]_2$ with 5,10,15-tris-pentafluorophenylcorrole (H_3tpfc), followed by treatment with tma-*N*-oxide.[21] Treatment of **1-Ir(tma)$_2$** with elemental bromine in methanol yielded an octabromo complex (Br_8-tpfc)Ir(tma)$_2$ (**1b-Ir(tma)$_2$**, Figure 1); both iridium(III) derivatives were characterized by nuclear magnetic resonance (NMR) spectroscopy, mass spectrometry (MS), X-ray crystallography, UV−vis spectroscopy, and cyclic voltammetry (CV). The planar macrocyclic framework in both **1-Ir(tma)$_2$** and **1b-Ir(tma)$_2$** is quite unlike that of porphyrins, which tend to saddle or ruffle when brominated.[22] In addition, the electrochemical data suggested that the metal, rather than the macrocycle, is oxidized to Ir(IV) in both complexes, in contrast with recent findings for analogous cobalt(III) corroles.[23]

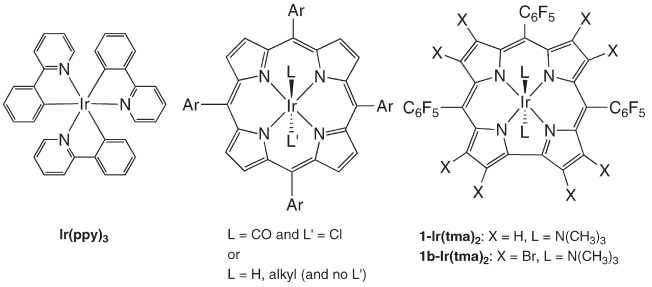

Figure 1. Complexes of 2-phenylpyridine, porphyrins, and corroles with iridium(III).

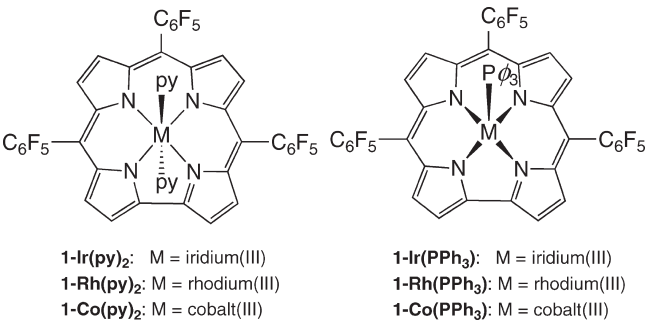

Figure 2. Axially ligated metal(III) corroles (py = pyridine).

Here we report the synthesis and characterization of corroles **1-Ir(py)$_2$** and **1-Ir(PPh$_3$)**, whose properties are compared with those of isostructural cobalt(III) and rhodium(III) analogues **1-Co(py)$_2$**, **1-Rh(py)$_2$**, **1-Co(PPh$_3$)**, and **1-Rh(PPh$_3$)** (Figure 2). Each set, **1-M(py)$_2$** or **1-M(PPh$_3$)**, represents a rare example of an entire transition metal group with the same oxidation state and coordination number, another being the Group 8 (por)M-CO series.[24] Our research has focused on the substitutional lability of Group 9 metallocorroles and the sites of oxidation reactions, as both change markedly within the group. We have found the following: Co(III) corroles are far more substitutionally labile than analogous Rh(III) or Ir(III) derivatives; the affinity of five-coordinate **1-M(PPh$_3$)** for a sixth ligand increases dramatically down the row; and oxidation of **1-M(py)$_2$** occurs primarily on the metal rather than on the macrocyclic ligand only in the case of iridium ($Ir^{III/IV}$). We report extensive electronic absorption, electrochemical, and electron paramagnetic resonance (EPR) data that support these conclusions.

Experimental Section

Materials. Silica gel for column chromatography (Silica Gel 60, 63−200 μm mesh) was obtained from EMD Chemicals, as were all solvents (tetrahydrofuran (THF), toluene, CH_2Cl_2, hexanes, and methanol). Most starting materials for syntheses were from Sigma-Aldrich and used without further purification. Exceptions are pyrrole and pentafluorobenzaldehyde, which were both purified by vacuum distillation before use. Tetrabutylammonium hexafluorophosphate, which was used as a supporting electrolyte in the CV experiments, was also from

(15) Saltsman, I.; Simkhovich, L.; Balazs, Y.; Goldberg, I.; Gross, Z. *Inorg. Chim. Acta* **2004**, *357*, 3038–3046.
(16) Luobeznova, I.; Raizman, M.; Goldberg, I.; Gross, Z. *Inorg. Chem.* **2006**, *45*, 386–394.
(17) Tse, M. K.; Zhang, Z.; Mak, T. C. W.; Chan, K. S. *Chem. Commun.* **1998**, 1199–1200.
(18) Palmer, J. H.; Day, M. W.; Wilson, A. D.; Henling, L. M.; Gross, Z.; Gray, H. B. *J. Am. Chem. Soc.* **2008**, *130*, 7786–7787.
(19) (a) Gryko, D. T.; Fox, J. P.; Goldberg, D. P. *J. Porphyrins Phthalocyanines* **2004**, *8*, 1091–1105. (b) Goldberg, D. P. *Acc. Chem. Res.* **2007**, *40*, 626–634. (c) Kerber, W. D.; Goldberg, D. P. *J. Inorg. Biochem.* **2006**, *100*, 838–857. (d) Aviv, I.; Gross, Z. *Chem. Commun.* **2007**, 1987–1999. (e) Ghosh, A.; Steene, E. *J. Inorg. Biochem.* **2002**, *91*, 423–436. (f) Kadish, K. M.; Shen, J.; Fremond, L.; Chen, P.; El Ojaimi, M.; Chkounda, M.; Gros, C. P.; Barbe, J. M.; Ohkubo, K.; Fukuzumi, S.; Guilard, R. *Inorg. Chem.* **2008**, *47*, 6726–6737.
(20) (a) Cheung, C. W.; Chan, K. S. *Organometallics* **2008**, *27*, 3043–3055. (b) Li, B.; Chan, K. S. *Organometallics* **2008**, *27*, 4034–4042. (c) Cui, W.; Li, S.; Wayland, B. B. *J. Organomet. Chem.* **2007**, *692*, 3198–3206. (d) Yanagisawa, M.; Tashiro, K.; Yamasaki, M.; Aida, T. *J. Am. Chem. Soc.* **2007**, *129*, 11912–11913. (e) Song, X.; Chan, K. S. *Organometallics* **2007**, *26*, 965–970. (f) Deng, Y.; Huang, M.-J. *Chem. Phys.* **2006**, *321*, 133–139. (g) Toganoh, M.; Konagawa, J.; Furuta, H. *Inorg. Chem.* **2006**, *45*, 3852–3854. (h) Flamigni, L.; Marconi, G.; Dixon, I. M.; Collin, J.-P.; Sauvage, J.-P. *J. Phys. Chem. B* **2002**, *106*, 6663–6671. (i) Zhai, H.; Bunn, A.; Wayland, B. *Chem. Commun.* **2001**, 1294–1295. (j) Shi, C.; Mak, K. W.; Chan, K. S.; Anson, F. C. *J. Electroanal. Chem.* **1995**, *397*, 321–324. (k) Collman, J. P.; Chng, L. L.; Tyvoll, D. A. *Inorg. Chem.* **1995**, *34*, 1311–1324. (l) Kadish, K. M.; Deng, Y. J.; Yao, C.-L.; Anderson, J. E. *Organometallics* **1988**, *7*, 1979–1983.
(21) Abbreviations: $[Ir(cod)Cl]_2$, H_3(tpfc), tpfc, Br_8-tpfc, *t*-4bpa, tma-N-oxide, tma, and py stand for iridium(I) cyclooctadiene chloride dimer, 5,10,15-tris-pentafluorophenylcorrole, 5,10,15-tris-pentafluorophenylcorrolato trianion, 2,3,7,8,12,13,17,18-octabromo-5,10,15-tris-pentafluorophenylcorrolato trianion, tris(4-bromophenyl)aminium hexachloroantimonate, trimethylamine N-oxide, trimethylamine, and pyridine, respectively.
(22) Ou, Z.; Shao, J.; D'Souza, F.; Tagliatesta, P.; Kadish, K. M. *J. Porphyrins Pthalocyanines* **2004**, *8*, 201–214, and references therein.
(23) Kadish, K. M.; Shen, J.; Fremond, L.; Chen, P.; El Ojaimi, M.; Chkounda, M.; Gros, C. P.; Barbe, J. M.; Ohkubo, K.; Fukuzumi, S.; Guilard, R. *Inorg. Chem.* **2008**, *47*, 6726–6737.
(24) Brown, G. M.; Hopf, F. R.; Meyer, T. J.; Whitten, D. G. *J. Am. Chem. Soc.* **1975**, *97*, 5385–5390.

Sigma-Aldrich and used without further purification. Electrodes for CV were obtained from CH Instruments.

Syntheses. The synthesis of 5,10,15-tris-pentafluorophenylcorrole (the H_3tpfc ligand) was accomplished by a simplified version of the standard procedure outlined in reference 1c.[25] The cobalt(III) and rhodium(III) corroles were available from previous studies.[15,26] Compounds **1-tma** and **2-tma** have only been reported in a previous communication,[18] hence their syntheses are summarized below along with those of the new corroles.

5,10,15-Tris-pentafluorophenylcorrolato-iridium(III) Bis-trimethylamine, 1-Ir(tma)$_2$. H_3tpfc (80 mg), $[Ir(cod)Cl]_2$ (335 mg), and K_2CO_3 (140 mg) were dissolved/suspended in 150 mL of degassed THF, and the mixture was heated at reflux under argon for 90 min (until corrole fluorescence was negligible to the eye upon long-wavelength irradiation with a hand-held lamp). Tma *N*-oxide (110 mg) was added, and the solution was allowed to slowly cool to room temperature while open to the laboratory atmosphere. Column chromatography of the black mixture (silica, 4:1 hexanes/CH_2Cl_2) provided an auburn solution, from which purple crystals of (tpfc)Ir(III)(tma)$_2$ (30 mg, 27% yield) could be grown by slow evaporation. ^{1}H NMR ($CDCl_3$): δ 8.90 (d, 2H, J = 4.2), 8.50 (d, 2H, J = 5.1), 8.38 (d, 2H, J = 4.5), 8.09 (d, 2H, J = 4.2), −2.95 (s, 18H). ^{19}F NMR ($CDCl_3$): δ −138.38 (m, 6F), −154.89 (m, 3F), −163.27 (m, 6F). MS (ESI): 1105.1 ([M$^+$]), 1046.0 ([M$^+$-tma]), 986.5 ([M$^+$-2tma]). UV−vis (CH_2Cl_2, nm, $\varepsilon \times 10^{-3}$ M^{-1} cm^{-1}): 388 (47), 412 (56), 572 (14), 640 (5.3).

2,3,7,8,12,13,17,18-Octabromo-5,10,15-tris-pentafluorophenylcorrolato-iridium(III) Bis-trimethylamine, 1b-Ir(tma)$_2$. Compound **1-Ir(tma)$_2$** (15 mg) and Br_2 (70 μL) were dissolved in 20 mL of MeOH and stirred overnight. Column chromatography (silica, 4:1 hexanes/CH_2Cl_2) of the red mixture provided a ruddy solution from which purple crystals of (Br_8-tpfc)Ir(III)(tma)$_2$ (15 mg, 63% yield) could be grown by addition of methanol followed by slow evaporation. ^{1}H NMR ($CDCl_3$): δ −2.60 (s, 18H). ^{19}F NMR ($CDCl_3$): δ −137.78 (d/d, 2F, ^3J = 35.1, ^4J = 18.3), −138.54 (d/d, 4F, ^3J = 33.9, ^4J = 17.1), −152.89 (m, 3F), −163.38 (m, 4F), −163.70 (m, 2F). MS (ESI): 1616.4 ([M$^+$ − 2tma]). UV−vis (CH_2Cl_2, nm, $\varepsilon \times 10^{-3}$ M^{-1} cm^{-1}): 404 (61), 424 (70), 580 (16), 654 (7.3).

5,10,15-Tris-pentafluorophenylcorrolato-iridium(III) Bis-pyridine, 1-Ir(py)$_2$. H_3tpfc (40 mg), $[Ir(cod)Cl]_2$ (170 mg), and K_2CO_3 (70 mg) were dissolved/suspended in 75 mL of degassed THF, and the mixture was heated at reflux under argon for 90 min. Pyridine (1 mL) was added, and the solution was allowed to slowly cool to room temperature while open to the laboratory atmosphere. Column chromatography of the forest green mixture (silica, 4:1 hexanes/CH_2Cl_2 followed by 3:2 hexanes/CH_2Cl_2) afforded a bright green solution, from which thin, green crystals of (tpfc)Ir(III)(py)$_2$ (26 mg, 50% yield) could be grown by addition of methanol followed by slow evaporation. ^{1}H NMR ($CDCl_3$): δ 8.84 (d, 2H, J = 4.5), 8.53 (d, 2H, J = 4.8), 8.32 (d, 2H, J = 4.8), 8.17 (d, 2H, J = 4.5), 6.21 (t, 2H, J = 7.8), 5.19 (t, 4H, J = 7.0), 1.72 (d, 4H, J = 5.1). ^{19}F NMR ($CDCl_3$): δ −138.68 (m, 6F), −154.84 (t, 2F, J = 22.2), −155.20 (t, 1F, J = 22.2), −163.28 (m, 4F), −163.65 (m, 2F). MS (ESI): 1144.1 ([M$^+$]). UV−vis (CH_2Cl_2, nm, $\varepsilon \times 10^{-3}$ M^{-1} cm^{-1}): 390 (28), 412 (43), 582 (12), 619 (6.5).

5,10,15-Tris-pentafluorophenylcorrolato-iridium(III) Triphenylphosphine, 1-Ir(PPh$_3$). H_3tpfc (40 mg), $[Ir(cod)Cl]_2$ (170 mg), and K_2CO_3 (70 mg) were dissolved/suspended in 75 mL of degassed THF, and the mixture was heated at reflux under argon for 90 min. Triphenylphosphine (260 mg dissolved in 5 mL THF) was added, and the solution was heated at reflux for another half hour under laboratory atmosphere before being allowed to cool to room temperature. Column chromatography of the deep green mixture (silica, 3:1 hexanes/CH_2Cl_2) afforded a bright red-orange solution, which could be evaporated to give (tpfc)Ir(III)(PPh_3) (30 mg, 64% yield) as a ruby-colored solid. ^{1}H NMR ($CDCl_3$): δ 8.67 (d, 2H, J = 4.5), 8.36 (d, 2H, J = 5.1), 8.18 (d, 2H, J = 5.1), 8.00 (d, 2H, J = 4.5), 6.98 (t, 3H, J = 7.2), 6.69 (t, 6H, J = 6.9), 4.52 (d/d, 6H, ^3J = 19.5, ^4J = 3.6). ^{19}F NMR ($CDCl_3$): δ −137.44 (m, 6F), −154.05 (m, 3F), −162.54 (m, 3F). MS (ESI): 1248.1 ([M$^+$]). UV−vis (CH_2Cl_2, nm, $\varepsilon \times 10^{-3}$ M^{-1} cm^{-1}): 398 (66), 554 (8.8), 588 (6.7).

Nuclear Magnetic Resonance Spectroscopy. ^{1}H and ^{19}F NMR data were obtained on $CDCl_3$ solutions of each compound at room temperature using a Varian Mercury 300 MHz NMR spectrometer. ^{1}H chemical shifts are reported relative to solvent peaks and ^{19}F chemical shifts are reported relative to a saved, external $CFCl_3$ standard.

Mass Spectrometry. Measurements were made on CH_3OH solutions of each compound by electrospray ionization into a Thermofinnigan LCQ ion trap mass spectrometer.

X-ray Crystallography. Concentrated CH_2Cl_2/CH_3OH solutions of corroles **1-Ir(tma)$_2$**, **1b-Ir(tma)$_2$**, and **1- Ir(py)$_2$** were allowed to undergo slow evaporation from scintillation vials. The resultant crystals were mounted on a glass fiber using Paratone oil and then placed on a Bruker Kappa Apex II diffractometer under a nitrogen stream at 100 K. The SHELXS-97 program was used to solve the structures.

Cyclic Voltammetry. CV measurements were made with a WaveNow USB Potentiostat/Galvanostat (Pine Research Instrumentation) using Pine AfterMath Data Organizer software. A three electrode system consisting of a platinum wire working electrode, a platinum wire counter electrode, and an Ag/AgCl reference electrode, was employed. The CV measurements were made using dichloromethane solutions, 0.1 M in tetrabutylammonium perchlorate (TBAP, Fluka, recrystallized twice from absolute ethanol), and 10^{-3} M substrate under an argon atmosphere at ambient temperature. The scan rate was 0.1 V/s and the $E_{1/2}$ value for oxidation of ferrocene under these conditions was 0.55 V.

UV−visible spectroelectrochemical measurements were made on dichloromethane solutions, 0.5 M in TBAP, and 0.1−0.3 mM in substrate with an optically transparent platinum thin-layer electrode working electrode, a platinum wire counter electrode, and an Ag/AgCl reference electrode under an argon atmosphere at ambient temperature. Potentials were applied with a WaveNow USB Potentiostat/Galvanostat. Time-resolved UV−visible spectra were recorded with a Hewlett-Packard Model 8453 diode array rapid-scanning spectrophotometer.

EPR Spectroscopy. Solutions for EPR were prepared by adding 50 μL of a 10 mM CH_2Cl_2 solution of iodine to 100 μL of a 1 mM CH_2Cl_2 solution of the corrole being examined, ensuring complete one-electron oxidation of the substrate. To rule out side reactions with iodine, sub-stoichiometric amounts of the radical cation tris(4-bromophenyl)aminium hexachloroantimonate (***t*-4bpa**) also were employed for oxidations. Spectra taken of the products obtained from reactions with both oxidants were virtually identical. EPR spectroscopy was performed using a Bruker EMX Biospin instrument, with a Gunn diode microwave source. Solutions were pre-cooled by rapid freezing in liquid nitrogen; spectra of samples at 20 K were obtained using liquid helium as a coolant. The SPINCOUNT package was used to simulate EPR parameters.[27]

(25) A 140 μL portion of a solution of 0.5 mL of trifluoroacetic acid in 5 mL of CH_2Cl_2 was added to 1.73 mL of warm (liquid) pentafluorobenzaldehyde, with rapid stirring. Addition of 1.46 mL of freshly distilled pyrrole resulted in the rapid formation of a viscous red solution. After 10 min, 20 mL of CH_2Cl_2 was added and the mixture was allowed to stir briefly, followed by slow addition of 3.84 g of DDQ to oxidize the newly formed macrocycle. Purification was accomplished by successive chromatographic treatments with 6.5:3.5 CH_2Cl_2/hexanes and 8.5:1.5 CH_2Cl_2/hexanes on silica, followed by recrystallization from hot pentane.

(26) (a) Simkhovich, L.; Galili, N.; Saltsman, I.; Goldberg, I.; Gross, Z. *Inorg. Chem.* **2000**, *39*, 2704–2705. (b) Mahammed, A.; Giladi, I.; Goldberg, I.; Gross, Z. *Chem.—Eur. J.* **2001**, *7*, 4259–4265.

(27) Golombek, A. P.; Hendrich, M. P. *J. Magn. Reson.* **2003**, *165*, 33–48.

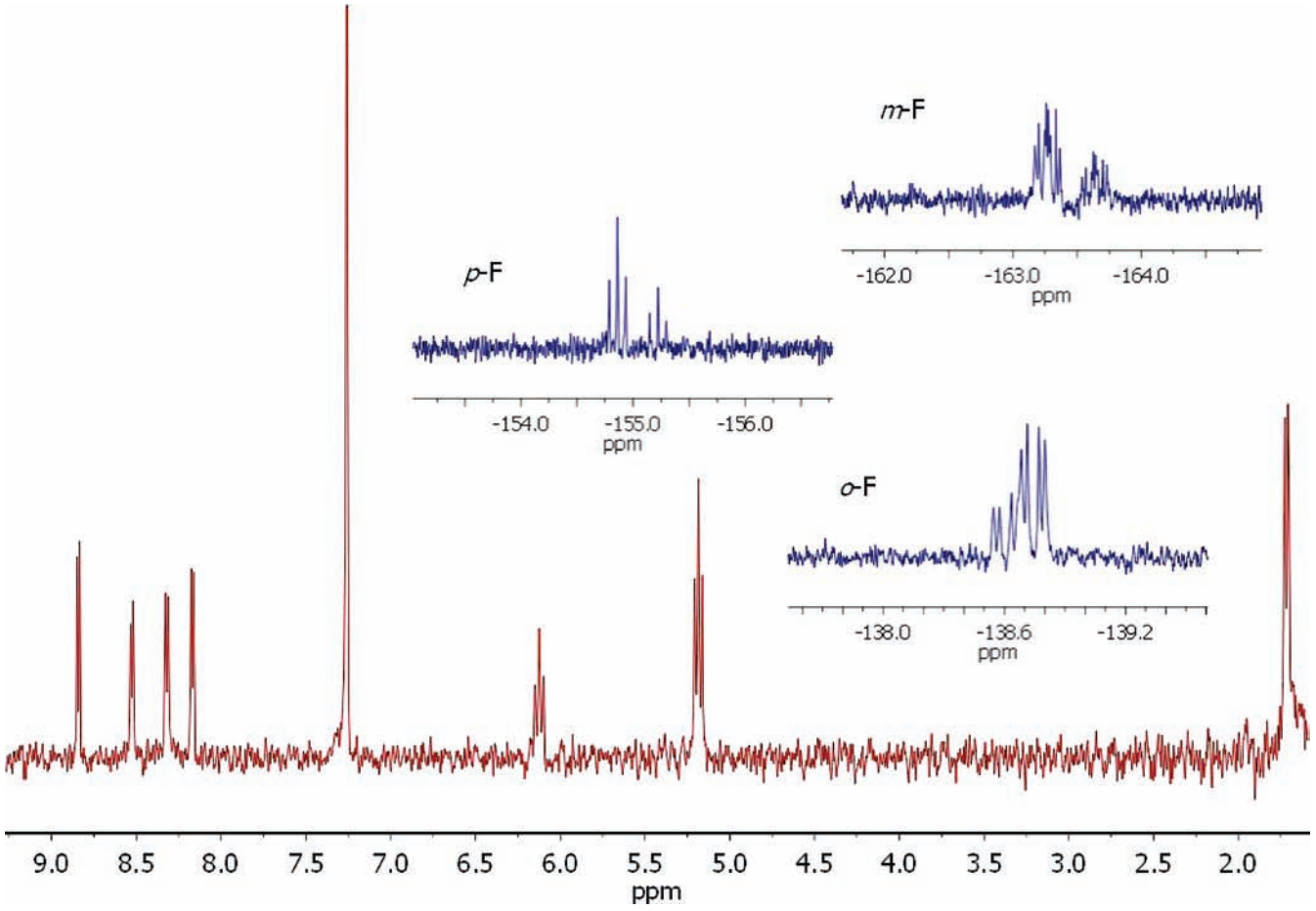

Figure 3. ^{1}H (red) and ^{19}F (blue inserts) NMR spectra of **1-Ir(py)$_2$**.

UV−vis Absorption Spectroscopy. Absorption spectral measurements were made on solutions of each compound in CH_2Cl_2, using a Hewlett-Packard 8452A Diode Array Spectrophotometer. Extinction coefficients were calculated from measurements on corroles at variable concentrations in CH_2Cl_2 solutions. UV−vis spectroscopic titrations were performed by stepwise addition of small aliquots of CH_2Cl_2 solutions of ***t*-4bpa** to CH_2Cl_2 solutions of each corrole. The ***t*-4bpa** oxidant was employed rather than iodine owing to overlapping absorptions because of excess reagent in the latter case.

Results and Discussion

Iridium(III) Corroles. The insertion of the metal ion into the free base corrole H_3(tpfc) was achieved via heating with $[Ir(cod)Cl]_2$ and K_2CO_3 in THF under an inert atmosphere. This procedure was followed by addition of pyridine or triphenylphosphine and opening the reaction mixture to the laboratory atmosphere to effect aerobic oxidation (see Supporting Information). Owing to their low-spin d^6 electronic configurations, iridium(III) corroles display highly resolved NMR spectra that are characteristic of diamagnetic complexes,[28] as shown in Figure 3 for **1-Ir(py)$_2$**. The ^{1}H NMR spectra reveal four β-pyrrole CH proton resonances as doublets with J coupling constants of about 4.5 Hz at 8−9 ppm and axial ligand resonances at high field attributable to the diamagnetic ring current of the aromatic corrole. The **1-Ir(py)$_2$** pyridine proton resonances are more shifted than those of PPh_3 in **Ir(PPh$_3$)** (both relative to their positions in the absence of a metal center) because of the proximity of py protons to the corrole ring. The coordination number (six for the bis-pyridine complex **1-Ir(py)$_2$** and five for the triphenylphosphine complex **1-Ir(PPh$_3$)**) can be deduced from ^{1}H NMR spectra via integration of the relevant proton resonances. The same information can also be extracted from ^{19}F NMR spectra (Figure 3, inset), since the C_{2v} symmetry of **1-Ir(py)$_2$** requires equivalence of above- and below-plane *ortho*- and *meta*-fluorine atoms on each C_6F_5 ring.

The electronic absorption spectra of six-coordinate metal(III) corroles are shown in Figure 4. The spectra of **1-Co(py)$_2$** and **1-Rh(py)$_2$** are similar, each with one major Soret band and Q bands near 580 and 600 nm, whereas the spectrum of **1-Ir(py)$_2$** exhibits highly structured Soret absorption with Q bands that are red-shifted by about 20 nm compared to those of the 3d and 4d analogues. We emphasize that **1-Co(py)$_2$** is in equilibrium with the *mono*pyridine complex **1-Co(py)** in CH_2Cl_2 solution [which is not the case for **1-Rh(py)$_2$** or **1-Ir(py)$_2$**].[26b] The spectrum of **1-Co(py)$_2$** in 5% pyridine (where only the bis-ligated form exists in solution) is in the Supporting Information. As the main components of the electronic spectra are attributable to corrole-based $\pi-\pi^*$ transitions in all cases, the differences likely reflect

(28) Balazs, Y. S.; Saltsman, I.; Mahammed, A.; Tkachenko, E.; Golubkov, G.; Levine, J.; Gross, Z. *Magn. Reson. Chem.* **2004**, *42*, 624–635.

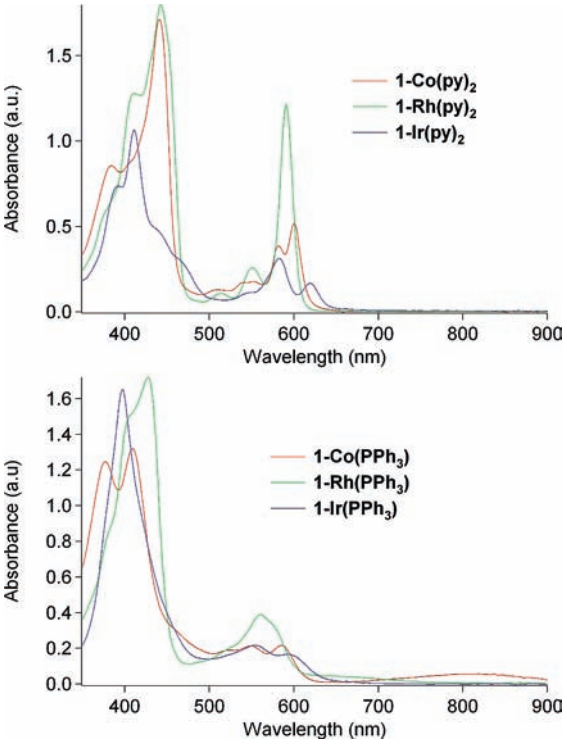

Figure 4. Electronic absorption spectra of six-coordinate bis-pyridine metal(III) corroles (top) and five-coordinate PPh_3-ligated metal(III) corroles (bottom); 2.5 μM in CH_2Cl_2 solution.

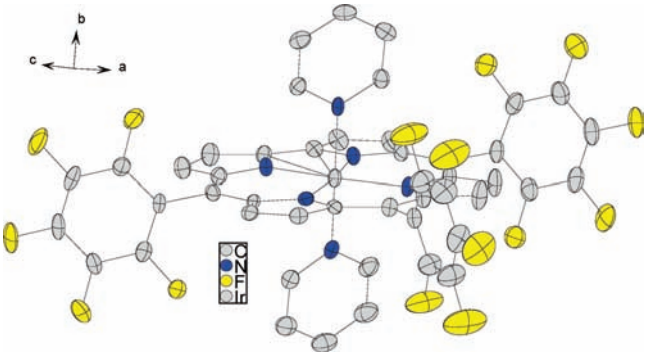

Figure 5. Structure of **1-Ir(py)$_2$** (H atoms omitted).

Table 1. Metal−Nitrogen Bond Lengths (Å) in **1-Co(py)$_2$**, **1-Rh(py)$_2$**, **1-Ir(py)$_2$**, **1-Ir(tma)$_2$**, and **1b-Ir(tma)$_2$**

	M−N(corrole)	M−N(axial)	reference
1-Co(py)$_2$	1.873(4)−1.900(4)	1.994(4)−1.995(4)	26b
1-Rh(py)$_2$	1.938(5)−1.976(5)	2.060(5)−2.071(5)	15
1-Ir(py)$_2$	1.947(2)−1.979(2)	2.052(2)−2.066(2)	this work
1-Ir(tma)$_2$	1.940(3)−1.981(3)	2.184(3)−2.186(3)	18
1b-Ir(tma)$_2$	1.959(2)−1.989(2)	2.186(2)−2.192(2)	18

increased mixing with MLCT in the order Co < Rh < Ir. Red-shifted Q bands also are exhibited by five-coordinate **1-Ir(PPh$_3$)**, while the Soret bands differ markedly, as follows: **1-Co(PPh$_3$)** has a highly split system, **1-Rh(PPh$_3$)** displays less splitting but is red-shifted, and **1-Ir(PPh$_3$)** exhibits a single, relatively sharp Soret band.

The structures of **1-Ir(tma)$_2$** and **1b-Ir(tma)$_2$** have been reported previously.[18] The newly obtained structure of **1-Ir(py)$_2$** [Crystallographic data have been deposited at the CCDC, 12 Union Road, Cambridge CB2 1EZ, U.K. and copies can be obtained on request, free of charge, by quoting the publication citation and the deposition number 657603.] is very similar to those of fully characterized **1-Co(py)$_2$** and **1-Rh(py)$_2$** analogues.[26b] **1-Ir(py)$_2$** has a planar macrocyclic framework (root-mean-square atomic deviation of 0.04 Å out of the plane defined by the N4 coordination core) with an in-plane Ir(III) and two virtually parallel axial pyridines (Figure 5). The axial Ir−N bond lengths of **1-Ir(py)$_2$** are much shorter than those of **1-Ir(tma)$_2$**, likely reflecting the π-acceptor capability of the pyridine ligands. **1-Ir(py)$_2$** and **1-Rh(py)$_2$** have similar M−N bond lengths; those of **1-Co(py)$_2$** are slightly shorter (Table 1).

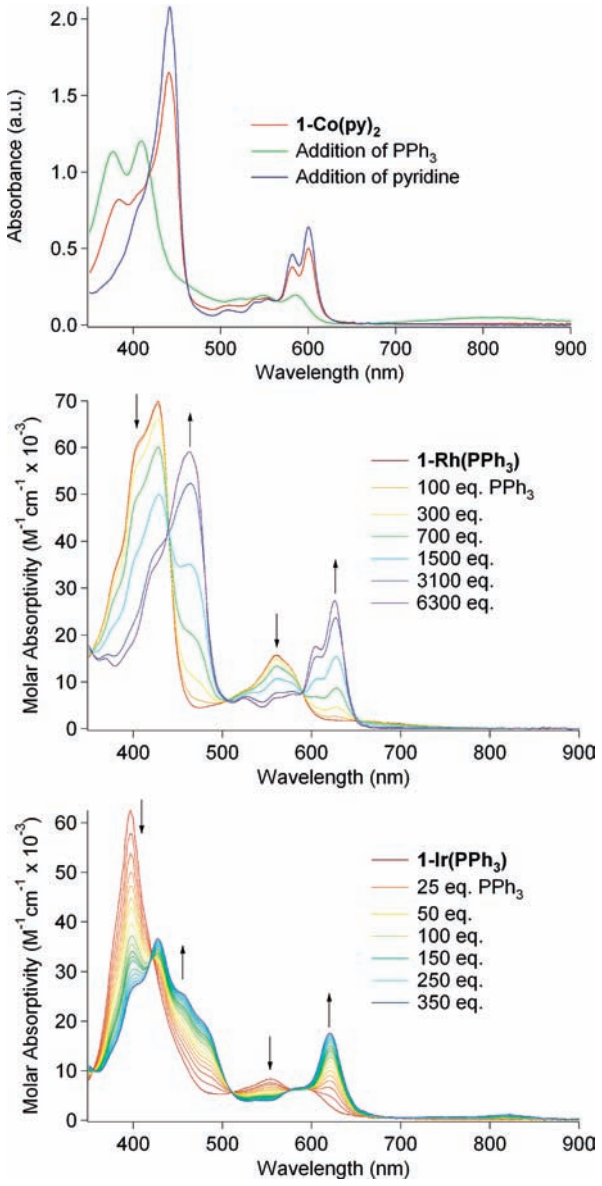

Figure 6. Electronic absorption spectra of metal(III) corroles in CH_2Cl_2 solution demonstrate: (a, top), reversible transformations between **1-Co(py)$_2$** and **1-Co(PPh$_3$)** upon addition of PPh_3 and pyridine; (b, middle), formation of **1-Rh(PPh$_3$)$_2$**; (c, bottom), formation of **1-Ir(PPh$_3$)$_2$**. Only a representative selection of the many individual traces (25 to 350 eq. ligand) that are shown in the bottom panel are specifically identified.

Substitution and Addition Reactions. Previous investigations have revealed that **1-Co(PPh$_3$)** and **1-Rh(PPh$_3$)**

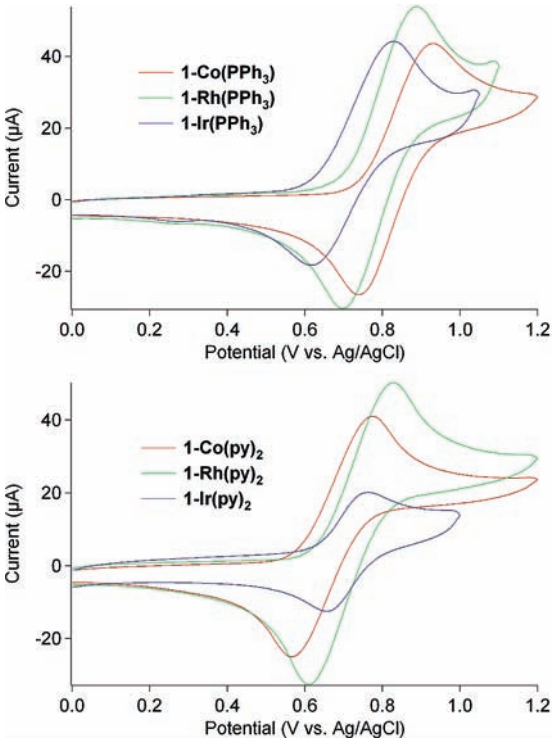

Figure 7. Cyclic voltammograms: (a, top) **1-M(PPh$_3$)**; (b, bottom) **1-M(py)$_2$**, in CH_2Cl_2 solutions.

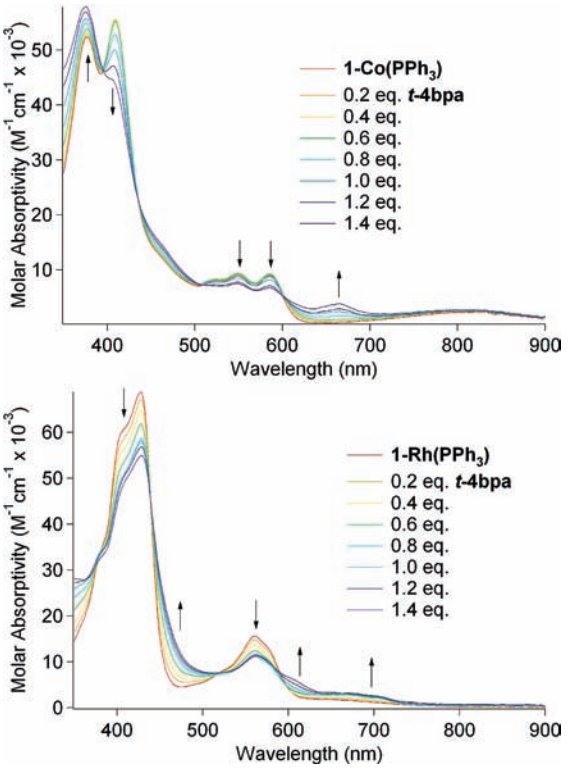

Figure 8. Absorption spectral changes accompanying oxidation of **1-Co(PPh)$_3$** (top) and **1-Rh(PPh)$_3$** (bottom) by ***t*-4bpa** in CH_2Cl_2 solutions.

Table 2. Reduction Potentials (CH_2Cl_2, TBAP, V vs Ag/AgCl) for Group 9 Metal(III) Corroles[a]

1-M(PPh$_3$)$_2$	$E_{1/2}$	**1-M(py)$_2$**	$E_{1/2}$
M = Co	0.83	M = Co	0.67
M = Rh	0.79	M = Rh	0.72
M = Ir	0.72	M = Ir	0.71

[a] Under virtually identical conditions, $E_{1/2}$ for ferrocene is 0.55 V; and iodine has E_{pa} of 0.89 V and E_{pc} of 0.39 V.

react differently with pyridine: both ligand substitution and addition to Co(III) yield **1-Co(py)$_2$**, but Rh(III) undergoes only addition to give **1-Rh(PPh$_3$)(py)**.[26b,29] The reactivity of **1-Ir(PPh$_3$)** is similar to that of Rh(III), that is, addition of pyridine produces a mixed-ligand complex (see Supporting Information). Additional confirmation of the substitutional lability of the Co(III) corrole is the observation (Figure 6a) that addition of PPh_3 to **1-Co(py)$_2$** rapidly yields **1-Co(PPh$_3$)** [addition of excess pyridine regenerates the bis-pyridine complex; the spectrum changes slightly because of the absence of 5-coordinate **1-Co(py)** under these conditions]. Complementary information was obtained by examination of spectral changes upon the addition of PPh_3 to five-coordinate metallocorroles. While addition of a 100,000-fold excess of triphenylphosphine produced only minor changes in the spectrum of **1-Co(PPh$_3$)** (see Supporting Information), the spectra of **1-Rh(PPh$_3$)** (Figure 6b) and **1-Ir(PPh$_3$)** (Figure 6c) changed completely after the addition of 6300 and 350 equiv, respectively. The similarity of the visible spectra obtained upon addition of triphenylphosphine to **1-Rh(PPh$_3$)** and **1-Ir(PPh$_3$)** to those of **1-Rh(py)$_2$** and **1-Ir(py)$_2$** suggests that the products are six-coordinate bis-triphenylphosphine species, **1-Rh(PPh$_3$)$_2$** and **1-Ir(PPh$_3$)$_2$**. While many corrole-chelated metal(III) ions possess surprisingly low affinities for a sixth ligand,[26b,30,31] our work demonstrates that this property is not as pronounced for 4d and especially for 5d metals.

Electrochemistry. Our earlier work focused on the differences between the β-pyrrole-unsubstituted complex **1-Ir(tma)$_2$** and its fully brominated analogue, **1b-Ir(tma)$_2$**. The latter displays one oxidation (at 1.19 V vs SCE) and one reduction (at −1.21 V vs SCE) within the solvent potential window of CH_2Cl_2, while two reversible oxidations (at 0.66 and 1.28 V vs SCE) were observed for the former.[18] The current emphasis is on the **M(+/0)** reduction potential of each of the complexes, because it should correspond to either a metal-centered (M^{III}/M^{IV}, where M = Co, Rh, or Ir) or a ligand-centered (tpfc/tpfc$^{+\bullet}$) process. The CVs of all complexes are shown in Figure 7; and Table 2 lists the corresponding reduction potentials. The results reveal that six-coordinate **1-M(py)$_2$** complexes are oxidized at lower potentials than five-coordinate **1-M(PPh$_3$)** and that the differences become larger in the order Ir < Rh < Co. It is surprising that there are only very small differences in reduction potentials for the two series: 0.70 ± 0.03 for **1-M(py)$_2$** and 0.78 ± 0.06 for **1-M(PPh$_3$)**. Very large potential shifts would be expected for metal-based processes ($M^{III/IV}$), as documented by the finding that $Rh^{III/IV}$ reduction potentials are 0.2 to

(29) Simkhovich, L.; Goldberg, I.; Gross, Z. *J. Porphyrins Phthalocyanines* **2002**, *6*, 439–444.

(30) Bendix, J.; Dmochowski, I. J.; Gray, H. B.; Mahammed, A.; Simkhovich, L.; Gross, Z. *Angew. Chem., Int. Ed.* **2000**, *39*, 4048–4051.

(31) Kowalska, D.; Liu, X.; Tripathy, U.; Mahammed, A.; Gross, Z.; Hirayama, S.; Steer, R. P. *Inorg. Chem.* **2009**, *48*, 2670–2676.

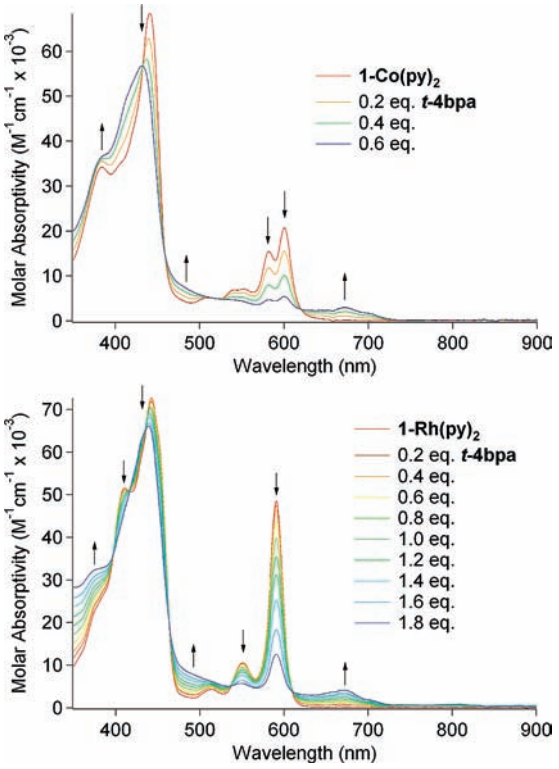

Figure 9. Absorption spectral changes accompanying oxidation of **1-Co(py)$_2$** (top) and **1-Rh(py)$_2$** (bottom) by ***t*-4bpa** in CH_2Cl_2 solutions. Reaction with the Co(III) complex was terminated after addition of 0.6 equiv, owing to product instability.[26b]

0.3 V more positive than $Ir^{III/IV}$ potentials in cyclometalated complexes.[32] A caveat is that the central metal ion should have some effect on the potential even in the case of macrocycle-centered oxidation, as observed previously for both corroles and porphyrins.[33,34]

Electronic Structures of One-Electron-Oxidized Metallo(III) Corroles. Changes in electronic spectra upon M(III) corrole oxidation can used as a tool for analyzing whether an electron is removed primarily from a metal or ligand orbital. One-electron oxidation of **1-Co(PPh$_3$)** or **1-Rh(PPh$_3$)** by ***t*-4bpa** (Figure 8) was marked by substantial intensity reductions of the M(III) Soret and Q bands and formation of a broad absorption system at 690 (ε = 4000 M^{-1} cm^{-1}) for cobalt and 710 nm (ε = 2300 M^{-1} cm^{-1}) for rhodium. These long-wavelength absorption features, which appear at 673 nm (ε = 3000 M^{-1} cm^{-1} for Co and 4100 M^{-1} cm^{-1} for Rh) in the spectra of chemically oxidized **1-Co(py)$_2$** and **1-Rh(py)$_2$** complexes (Figure 9), represent signature spectroscopic features for corrole-centered oxidations.

Absorption spectral changes upon oxidation of iridium(III) corroles are substantially different from those of 3d and 4d analogues. Oxidations of **1-Ir(PPh$_3$)**, **1-Ir(py)$_2$**, and **1-Ir(tma)$_2$** by ***t*-4bpa** in CH_2Cl_2 were performed, and their progress was tracked by UV−visible spectroscopy (Figure 10). In the case of the five-coordinate complex **1-Ir(PPh$_3$)**, oxidation causes a significant

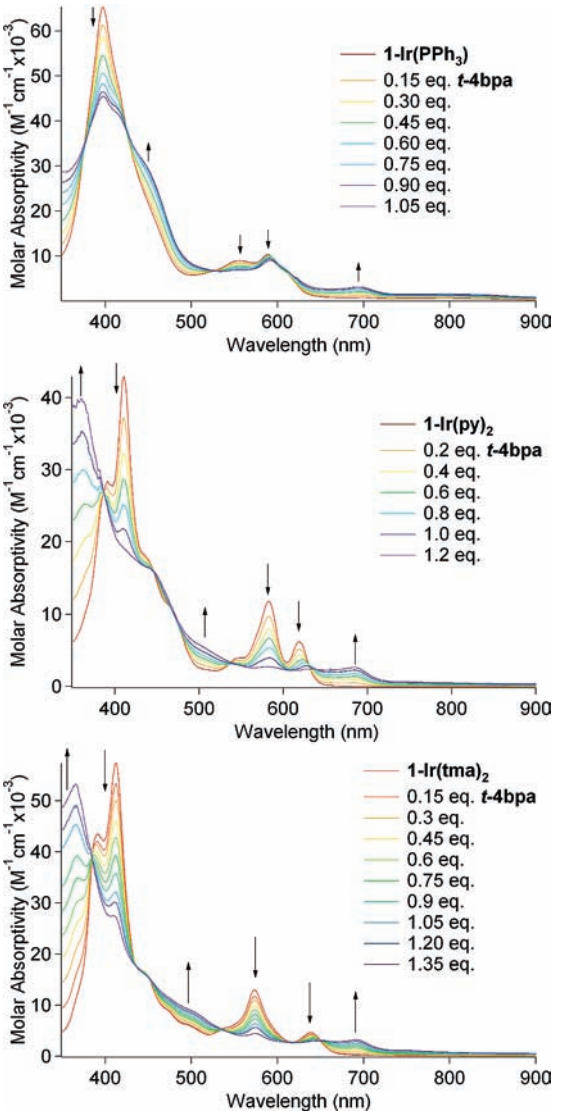

Figure 10. Absorption spectral changes accompanying oxidation of **1-Ir(PPh$_3$)** (top), **1-Ir(py)$_2$** (middle), and **1-Ir(tma)$_2$** by ***t*-4bpa**.

reduction in the intensity of the Soret system, accompanied by broadening, and the Q-bands are slightly red-shifted. For each of the six-coordinate complexes **1-Ir(py)$_2$** and **1-Ir(tma)$_2$**, the Soret band blue shifts over 30 nm (peaks at 366 nm) and the Q-bands all but vanish. A weak absorption appears at 695 nm (ε = 3000 M^{-1} cm^{-1}) in the spectrum of **1-Ir(PPh$_3$)**; and a similar system is centered at 685 nm (ε = 2600 M^{-1} cm^{-1}) in the spectra of the six-coordinate complexes; these features are red-shifted from the 673 nm band observed upon oxidation of either **1-Co(py)$_2$** or **1-Rh(py)$_2$**, suggesting that the site of oxidation is different for Ir(III). As it is well established that substantial blue shifts of Soret bands accompany metal-centered oxidations [Note that a 32 nm blue shift in the Soret peak occurs upon oxidation of [**1-Cr^{IV}(O)**]$^-$ to [**1-Cr^{V}(O)**] (see ref 35).] of metallocorroles,[5b,35] an Ir(IV) oxidation state is indicated for each of the one-electron-oxidized Ir(III) complexes.

(32) Calogero, G.; Giufridda, G.; Serroni, S.; Ricevuto, V.; Campagna, S. *Inorg. Chem.* **1995**, *34*(3), 541–545.
(33) Gross, Z. *J. Biol. Inorg. Chem.* **2001**, *6*, 733–738.
(34) Fuhrhop, J. H.; Kadish, K. M.; Davis, D. G. *J. Am. Chem. Soc.* **1973**, *95*, 5140–5147.
(35) Meier-Callahan, A. E.; di Bilio, A. J.; Simkhovich, L.; Mahammed, A.; Goldberg, I.; Gray, H. B.; Gross, Z. *Inorg. Chem.* **2001**, *40*, 6788–6793.

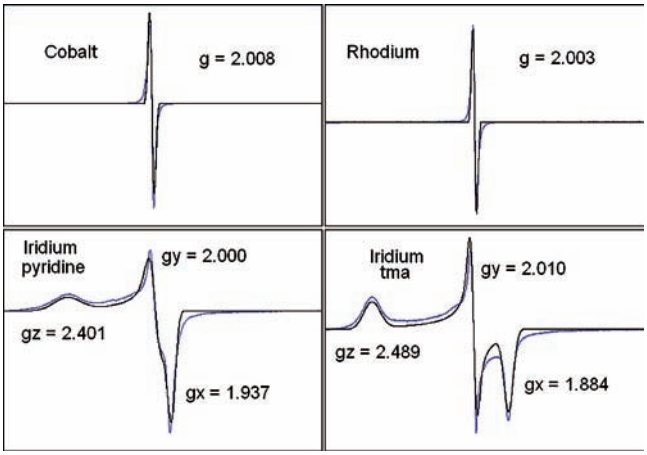

Figure 11. EPR spectra taken at 20 K in frozen toluene solutions (CH_2Cl_2 was added to Co and Rh toluene solutions with ***t*-4bpa**) of the chemically oxidized forms of (clockwise from top left): (a) 1-Co(py)$_2$; (b) 1-Rh(py)$_2$; (c) 1-Ir(tma)$_2$; (d) 1-Ir(py)$_2$. The blue traces are experimental spectra; the black traces are simulations performed using the SPINCOUNT package.

EPR Spectra. Carbon-based organic radicals, such as those obtained from oxidation of corrole complexes with non-redox-active metals like gallium(III), exhibit EPR spectra with isotropic g values near 2.0023.[30] In stark contrast, low-spin d^5 metal complexes with organic ligands display highly anisotropic EPR signals, often with hyperfine splittings attributable to electron-nucleus interactions.[36]

Complexes **1-Co(py)$_2$**, **1-Rh(py)$_2$**, **1-Ir(py)$_2$**, and **1-Ir(tma)$_2$** were oxidized chemically with 5 equiv of elemental iodine in CH_2Cl_2, and EPR spectra of the resultant solutions were recorded at 20 K. Each of the spectra of the oxidized cobalt and rhodium complexes displays a single, narrow band [centered at g = 2.008 (Co, Figure 11a) or g = 2.003 (Rh, Figure 11b), respectively] clearly attributable to a corrole-based radical. Such a radical signature is not found in the EPR spectrum of either of the oxidized **1-Ir(py)$_2$** and **1-Ir(tma)$_2$** complexes. The oxidation product of **1-Ir(tma)$_2$** exhibits a highly rhombic spectrum (Figure 11c), with g tensor components (g_{zz} = 2.489, g_{yy} = 2.010 g_{xx} = 1.884) that are very similar to those of low-spin d^5 metalloporphyrinoids such as bis-amine-iron(III) porphyrins[37] and (tpfc)Fe(py)$_2$,[38] thereby demonstrating the presence of a bona fide iridium(IV) corrole. The spectrum of the product of oxidation of **1-Ir(py)$_2$** under the same conditions also is highly anisotropic, albeit with less rhombicity, with g_{zz} = 2.401, g_{yy} = 2.000, g_{xx} = 1.937 (Figure 11d).

Interpretation of the EPR spectra of oxidized five-coordinate complexes **1-Co(PPh$_3$)**, **1-Rh(PPh$_3$)**, and **1-Ir(PPh$_3$)** is problematic. Oxidized **1-Co(PPh$_3$)** and **1-Rh(PPh$_3$)** appear to be corrole radicals (with isotropic g tensors centered near the free-electron value), but the electronic structure of oxidized **1-Ir(PPh$_3$)** cannot be assigned, as its EPR spectrum is obscured by signals likely generated from side reactions with iodine.

Concluding Remarks

Our investigation is the first to focus on the reactivity patterns of an isostructural series of corrole-chelated transition metals. The results shed new light on the chemical reactivity and stability of high oxidation states of metallocorroles. There is a clear trend within each series in terms of ligand substitution (only cobalt(III) corroles appear labile at room temperature) and ligand addition to the five-coordinate **1-M(PPh$_3$)** (Co < Rh < Ir), whereas all complexes display similar reduction potentials. The unexpected insensitivity of reduction potentials to metal identity has been interpreted in terms of different centers of oxidation for each complex. Absorption and EPR spectral data demonstrate that the first oxidation is corrole-centered for cobalt and rhodium, but metal-centered for iridium. Our demonstration that the reactivity patterns of Ir(III) corroles are so different from those of 3d and 4d analogues suggests that increased efforts should be made to obtain complexes of other 5d metals, as it is likely that such materials will exhibit rich and in some cases unexpected physical and chemical properties that will further expand the range of useful applications for these electronically unique macrocycles.

Acknowledgment. This work was supported by the Center for Chemical Innovation Grant NSF CHE-0802907, U.S.−Israel BSF (Z.G. and H.B.G.), BP, CCSER (Gordon and Betty Moore Foundation), and the Arnold and Mabel Beckman Foundation. We thank Dr. Angelo Di Bilio for help with measurements of low-temperature EPR spectra; and Drs. Lawrence M. Henling and Michael W. Day for assistance with the acquisition and analysis of crystallographic data.

Supporting Information Available: Additional information as noted in the text. This material is available free of charge via the Internet at http://pubs.acs.org.

(36) (a) Diversi, P.; Iacoponi, S.; Ingrosso, G.; Laschi, F.; Lucherini, A.; Pinzino, C.; Ucello-Barretta, G.; Zanello, P. *Organometallics* **1995**, *14*, 3275–3287. (b) Diversi, P.; de Biani, F. F.; Ingrosso, G.; Laschi, F.; Lucherini, A.; Pinzino, C.; Ucello-Barretta, G.; Zanello, P. *J. Organomet. Chem.* **1999**, *584*, 73–86.

(37) Walker, F. A. *Coord. Chem. Rev.* **1999**, *185−186*, 471–534.

(38) Simkhovich, L.; Goldberg, I.; Gross, Z. *Inorg. Chem.* **2002**, *41*, 5433–5439.